Title: Wave Energy Extraction in the Northeast Atlantic: Future Wave Climate Availability

Author(s): Jelena Janjic[1], Sarah Gallagher[2] and Frederic Dias[1]

[1]UCD School of Mathematics and Statistics, University College Dublin, Ireland
[2]Research, Environment and Applications Division, Met Éireann, Dublin, Ireland

Citation: Janjic , J., S. Gallagher, F. Dias, 2017. “Wave Energy Extraction in the Northeast Atlantic: Future Wave Climate Availability”. In Proceedings of the 12th European Wave and Tidal Energy Conference EWTEC, 27th Aug – 1st Sept 2017, Cork, Ireland, pp. 870:1–9. ISSN 2309-1983.

Wave Energy Extraction in the Northeast Atlantic: Future Wave Climate Availability

Jelena Janjić
School of Mathematics & Statistics
University College Dublin
Belfield, Dublin 4, Ireland
E-mail: jelena.janjic@ucdconnect.ie

Sarah Gallagher
Research, Environment & Applications
Met Éireann
Glasnevin Hill, Dublin 9, Ireland
E-mail: sarah.gallagher@met.ie

Frédéric Dias
School of Mathematics & Statistics
University College Dublin
Belfield, Dublin 4, Ireland
E-mail: frederic.dias@ucd.ie

***Abstract*—To examine the long-term viability of wave energy extraction locations, we analyse how the wave energy resource of the Northeast Atlantic may change both annually and seasonally towards the end of the twenty first century, using a three-grid WAVEWATCH III (WW3) model ensemble. Two greenhouse gas emission scenarios or Representative Concentration Pathways (RCPs) RCP4.5 and RCP8.5 are analysed, with three members in each RCP wave model ensemble. We examine in detail the percentage of time for which energy extraction is possible, discounting sea states where the Wave Energy Converters (WECs) will be non-operational. This provides a useful analysis of locations around the coast of Ireland, Scotland and France not only where the most energetic wave climate can be found, but also the locations where WEC deployment is the most productive in terms of hours of potential operation of the WEC, compared to the total length of the observed period. The model is forced by EC-Earth data (10 m winds and sea ice fields). A hindcast driven by ERA-Interim fields is also produced for validation. Although a significant reduction in the overall wave energy flux towards the end of the century was found, the subsequent change in potential hours of operation remained stable.**

***Index Terms*—WAVEWATCH III; Northeast Atlantic; EC-Earth model; Climate projections; Wave Energy Converters.**

I. Introduction

The formation of waves is caused by the wind blowing over the surface of the sea. The height of these waves is a function of the wind speed, duration for which the wind blows, the distance of water over which wind blows (called the fetch), bathymetry of the seafloor (which can cause the energy of the waves to disperse or to focus) and currents. The world's oceans, covering three quarters of the earth surface, contain enormous quantities of unused wave renewable energy. Ireland is ideally positioned for ocean energy extraction with its exposure to the Atlantic Ocean [1]–[3]. Unfortunately, the challenges we encounter are an intermittent wave energy source, low performance of wave energy converters (WECs) during extreme sea states, a huge variety of WECs that are still not commercially viable [4], [5]. Furthermore, it should not be forgotten that WECs can potentially disturb the seabed, change the habitat of nearshore creatures and be a source of underwater noise that may affect sea life around them. Though wave energy has its challenges and shortcomings, wave energy is more concentrated in space than both wind and solar energy, abundant and more available compared to fossil fuels. Harnessing such energy has the potential to supply a significant part of electrical energy consumption and with the attention drawn to the rise of CO_2, electricity generation using renewable sources becomes a more and more important area of research [4]. To be able to capture wave energy, it is necessary to construct a WEC that can respond properly to the forces applied to it by waves. Parts of a WEC are allowed to move, so it can convert wave energy into mechanical energy and subsequently this energy is converted to electricity [6]. Depending on the principle they use to convert waves into mechanical energy, WECs can be classified into attenuators, point absorbers, oscillating wave surge converters, oscillating water columns, overtopping/terminators, submerged pressure differentials, bulge wave devices and rotating mass devices. They can also be categorized by location into shoreline, nearshore, and offshore devices [4], [7]. Though shoreline and nearshore devices have the advantage when it comes to maintenance and smaller probability of extreme wave events that may cause damage, they also experience lower wave energy compared to offshore devices. For high and uninterrupted performance the wave energy converter should be designed to withstand different wave climates. Depending on the wave climate we may expect different power outputs [8]. Not only does the power output depend on the wave climate but also the construction, maintenance, and survivability of WECs [4]. For this reason we should properly investigate the wave climate of the potential sites for WEC deployment. This study aims to produce detailed information on the wave climate and the severity of the extremes both annually and seasonally, to investigate the change that may occur by the end of the 21st century in different locations in the Northeast Atlantic and to clarify what can be reasonably expected as the mean output of WECs in the locations of interest (see Table I and Figure 1).

II. Model Details

A. EC-EARTH Model

EC-Earth model is one of a variety of Earth System models (EMS) [9] which are run under the CMIP5 [10] framework created to address scientific questions that arose as a part of the IPCC AR4 process (Intergovernmental Panel on Climate Change 4th Assessment Report). The EC-Earth model has

been chosen because the outputted mean sea level pressure, high wind speed, and extratropical cyclone characteristics compared well to the European Centre for Medium-Range Weather Forecast (ECMWF) ERA-Interim reanalysis data [11]. This EMS model version 2.3 consists of an atmosphere-land surface module coupled to an ocean-sea ice module [12], [13] with the Ocean Atmosphere Sea Ice Soil coupler (OASIS) version 3 [14]. The atmospheric component of this model is based on the Integrated Forecasting System with a spatial resolution of 125 km and 62 vertical layers up to 5 hPa. The oceanic component is the Nucleus for European Modelling of the Ocean version 2 with a resolution of 110 km [15] with 42 vertical layers and finally the Sea-Ice component is the Louvain-la-Neuve Sea Ice Model (LIM) version 2 [16].

Fig. 1. Three locations were examined in detail: Location 1 near the Atlantic Marine Energy Test site (AMETS) of the west coast of Ireland; Location 2 to the west of the European Marine Energy Centre (EMEC) off the Orkney's; and Location 3 to the west of SEM-REV marine test facility, France.

The EC-Earth model has been run with two future scenarios Representative Concentration Pathways (RCPs) RCP4.5 and RCP8.5, where RCP4.5 is medium/high stabilized at approximately 4.5 W/m^2 after 2100 and RCP8.5 is high pathway with a radiative forcing that reaches over 8.5 W/m^2 by year 2100 [17]. There are three realizations $(X = 1, 2, 3)$, each driven by a separate EC-Earth ensemble member, which make up the wave climate ensemble: each containing one historical (mei$X$) and two future simulations (me4X and me8X) corresponding

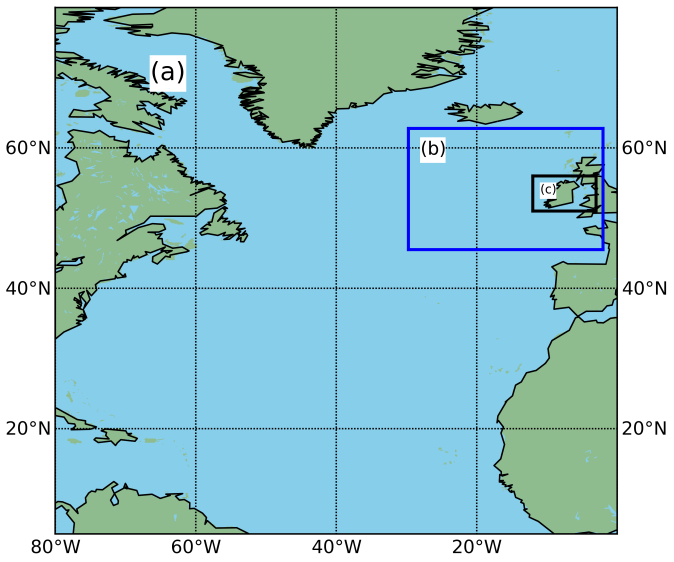

Fig. 2. The WAVEWATCH III model domains used in [19]. This study focuses on the middle grid b) shown by the blue box.

to the above mentioned RCPs. The historical period is from 1980 to 2009 and the future period is from 2070 to 2099. To conclude there are nine 30-year data sets and with the ERA-Interim hindcast, ten simulations in total.

B. WAVEWATCH III

WW3 [18] is a third generation phase-averaged model that solves the wave action balance equation where conservation of the action density is balanced by source terms that represent physical processes that generate or dissipate waves. The model has been forced with EC-Earth model 10 m winds and sea ice fields and ERA-Interim data. The model was run with three grids (see Figure 2). The grid a) covers the North Atlantic with a resolution of 0.75° x 0.75°. Grid b) covers the Northeast Atlantic with a resolution of approximately 25 km (0.25° x 0.25°). The grid around Ireland is an unstructured grid with a resolution from 15 km offshore to 1 km nearshore but was not the focus of this study. The focus of our analysis is on the middle grid (b), which covers a larger region in the Northeast Atlantic, as opposed to the grid only around the nearshore of Ireland (c), which was examined in [19] and [20], as this provides an opportunity to examine, in addition to Ireland, the west coast of Scotland and France as areas with high wave energy potential. This research studies the historical and future period of hourly outputted values over the Northeast Atlantic of the following wave parameters:

- Energy flux (W/m):

$$C_g E = \rho_w g \overline{C_g} E \tag{1}$$

where $\overline{C_g}$ denotes the averaged group velocity over the frequency-direction spectrum (see [18]), ρ_w water density

and g is the acceleration due to gravity. E denotes the first moment of the variance density spectra $F(f,\theta)$:

$$E = \int_0^{2\pi} \int_0^{\infty} F(f,\theta) df\, d\theta \tag{2}$$

- Peak period (s):

$$T_p = 1/f_p \tag{3}$$

where f_p denotes the peak frequency (Hz).

- Significant wave height (m):

$$H_s = 4\sqrt{E} \tag{4}$$

- Energy period(s):

$$T_{m0,-1} = 2\pi\overline{\sigma^{-1}} \tag{5}$$

where σ is a intrinsic radian frequency (for more details see [18]).

III. Methodology

WECs are highly sensitive to wave forces on the device: large amplitude waves can cause damage to the converter and small amplitude waves will not cause the movement of the mobile part of the device thus no power will be produced. When H_s is greater than 7 m, energy is considered to be non-extractable, while when H_s is smaller than 1 m, energy is considered to be too small to have a meaningful power output from the device. Indeed, when H_s is greater than 7 m, the waves can be potentially dangerous for the device. Time intervals when H_s is smaller than 1 m can be used for device maintenance [21]. Therefore, we have analysed the percentage of time when waves have been in the range from 1 to 7 m [22], [23]. Also, we were interested to see what part of the total available energy devices extract by using the above mentioned range, both annually and seasonally. Therefore, we chose this theoretical max/min as a realistic range for extractable power across all WEC technologies as one that is realistic for the safe extraction of wave power and a practical metric based on [22], [24], [25]. We acknowledge that we have taken a simplified approach in our study and that there are more factors to be considered in the wave interaction with the Wave Energy Converter. Nevertheless, we believe that it may provide useful information on the nature of any potential WEC installation site.

To be able to identify the annual and seasonal distribution of wave energy, a 10 year period is usually recommended to avoid the inter-annual wave fluctuations [26]. In fact the wave climate of the Northeast Atlantic varies on time scales of decades or more [27]. In this study we have used 3 x 30-year (so 90 years in total) hourly timeseries datasets to provide scatter diagrams (H_s,T_e) of the significant wave height (H_s) and wave period (T_e).

The relationship between the sea state and the WEC power output is presented as a table of different power values depending on H_s and T_e. These tables are known as power matrices and they can be obtained numerically or experimentally by the WEC manufacturer. The sea state is described by only two parameters H_s and T_e (or T_p) which is one of the limitations [8] of using power matrices to calculate the expected power output [28] because WECs respond to the spectral shape [29], [30]. We considered power matrices of five different WECs listed in Table II, taken from [24] and [31]. The power matrices were used to calculate the Annual Mean Absorbed Power (AMAP) using the scatter diagrams of wave data statistics [24] for different locations listed in Table I.

TABLE I
Location details

	Latitude (°N)	Longitude (°W)	Description
1	54.25	−10.5	near AMETS
2	59	−3.75	west of EMEC
3	47.25	−3.5	west of SEM REV

TABLE II
Wave Energy Converters

WEC	Principle	Maximum power (kW)	Depth (m)
Pelamis	Attenuator	750	>50
F-2HB	Point absorber	1000	>50
F-3OF	Oscillating flap	1665	Deep
F-OWC	Point absorber	2880	>100
F-HBA	Point absorber	3619	>100

To calculate AMAP we used the following equation [8]:

$$P_E = \frac{1}{100} \sum_{i=1}^{n_T} \sum_{j=1}^{n_H} p_{ij} P_{ij} \tag{6}$$

The probability of occurrence scatter diagrams and power matrices data can be considered as matrix elements p_{ij} and P_{ij}. Each element of the matrix corresponds to a combination of these indices but also to a combination of H_s and T_e. P_{ij} is the expected power that WEC will provide in a sea state characterised by the (H_s, T_e) corresponding to the (i,j) combination, while p_{ij} is the probability of occurrence of this sea state in the area of observation. The integers n_T and n_H represent the number of wave period and significant wave height bins in a power matrix respectively.

IV. Validation

The model was validated in [19] by comparing the historical EC-Earth WW3 runs and ERA-Interim hindcast. There was a small difference of 5% between the historical ensemble mean and the hindcast off the west coast (EC-Earth driven historical run over predicting wave heights compared to ERA-Interim driven hindcast for 30-year annual and seasonal averages). The ERA-Interim driven WW3 run was also compared to buoy

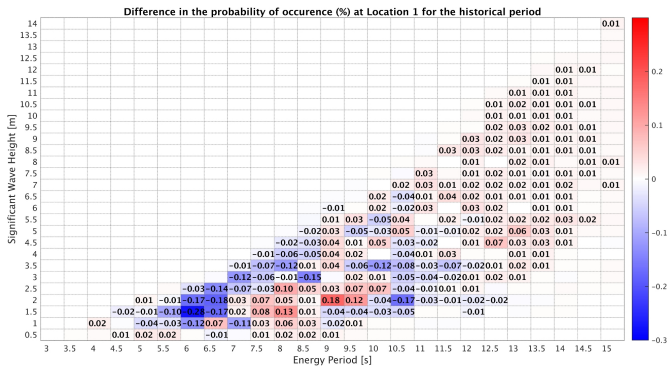

Fig. 3. Percentage difference in the frequency of occurrence of the hourly timeseries of H_s and T_e for the EC-Earth driven WW3 runs to that of the ERA-Interim WW3 hindcast, for Location 1 (AMETS), from 1980 - 2009.

measurements and showed good correlations to the buoy data. For further details see [19]. In addition, this was expanded by comparing the ERA-Interim driven WW3 run with the historical EC-Earth WW3 runs for the wave energy flux, by season in [32]. We have also compared the differences in the frequency of occurrence scatter plots of the hourly timeseries of H_s and T_e between the EC-Earth driven WW3 runs and the ERA-Interim hindcast at Location 1, as can be seen in Figure 3. Some differences can be seen in the lower H_s and T_e values, where there are more low energy sea-states in ERA-Interim driven WW3 runs. However, there is a slightly higher frequency of more energetic sea-states (higher H_s and T_e). It is interesting to note that athough the difference between the ERA-Interim driven WW3 and the historical EC-Earth WW3 runs is only 5%, there are slightly larger uncertainties when looking at different sea states that are partly balanced out while looking at the average. This is consistent with the validation carried out in [19], where there is a slight over prediction in H_s in the EC-Earth driven runs off the west coast.

V. Results

A. Projected Changes in Wave Energy Flux

Figure 4 displays the ensemble mean wave energy flux (C_gE is described in Equation 1), both annually and seasonally for the historical period 1980 - 2009, and the subsequent estimated percentage changes (%) for the future period 2070 - 2099 under the RCP4.5 and RCP8.5 scenarios. Ensemble mean is the mean of the values obtained from either past or future simulations from different ensemble members, e.g. future ensemble mean for RCP8.5 would be a mean of me81, me82, and me83. As can be seen in Figure 4, there is a general reduction in C_gE across all seasons, with the strongest relative decrease in summer (40%) and the largest decrease in absolute magnitude terms in winter (30 kW/m) off the west coast of Ireland and France. Decreases in spring and autumn are not as significant. In summer, in the north of the domain above Scotland, an area of statistically non-significant increase (12%) can be found related to the increase in the driving 10 m winds to the south of Iceland found in [19].

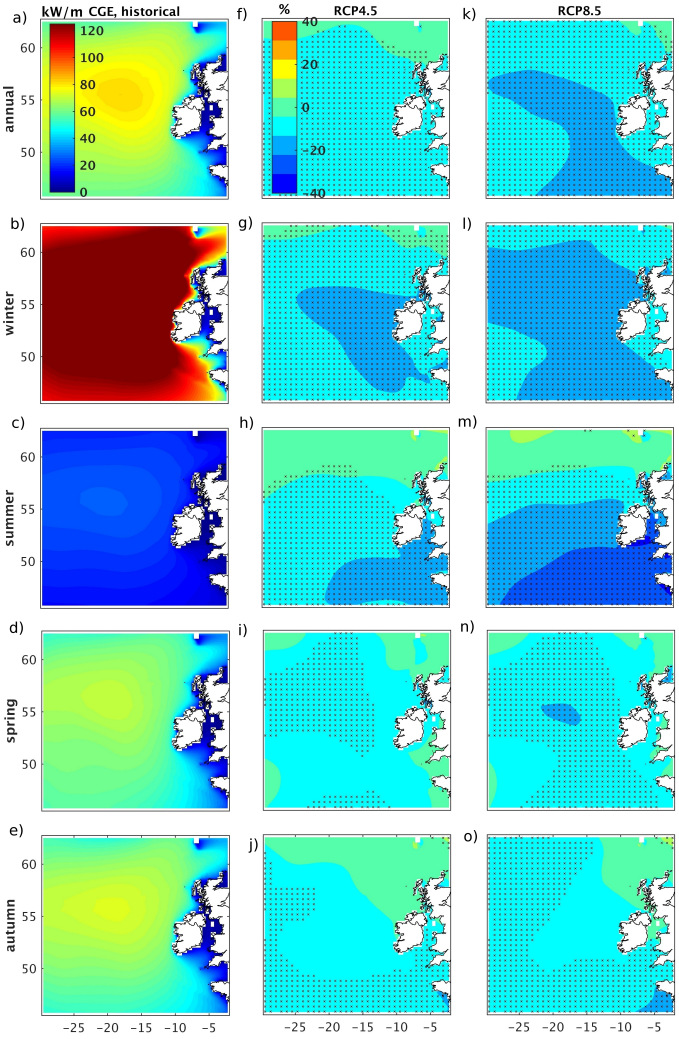

Fig. 4. Ensemble mean (a) annual, (b) winter, (c) summer, (d) spring, and (e) autumn C_gE (kW/m) for the historical period (1980-2009). Projected changes (%) of C_gE for the period 2070-2099 relative to 1980-2009 for RCP4.5 (f) annual ensemble mean, (g) winter, (h) summer, (i) spring, (j) autumn and for RCP8.5 (k) annual ensemble mean, (l) winter, (m) summer, (n) spring and (o) autumn ensemble mean. Stippling indicates where the % changes in the future C_gE ensemble mean exceed twice the inter-ensemble standard deviation.

B. Probability of Occurrence Scatter Diagrams

Figure 5 shows frequency of occurrence scatter diagrams of H_s and T_e, for the historical period (left panels) and the subsequent change under the RCP8.5 scenario for the future period (right panels). A map of the locations can be seen in Figure 1 and is described in Table I. There is a general decrease (blue) in the more energetic sea states (higher H_s and T_e) in Location 1 (near AMETS off the west coast of Ireland), and Location 3 (west of the SEM-REV marine test site, France) and an increase (red) in lower H_s and T_e sea states. This is consistent with Figure 4, where there are significant annual and seasonal decreases in C_gE in both of these regions. For Location 2 (west of EMEC, Scotland) a more complicated

picture emerges, with decreases in the high and low energy states, but an increase in the mid-ranges. Examining Figure 4 at Location 2 by season, only winter shows a statistically significant change in C_gE. Both the summer and autumn seasons show areas of neutral or increased wave energy flux. The projected seasonal change is considered significant in this study if the % changes in the future mean seasonal value of the parameter exceed twice the inter-ensemble standard deviation, similar to the metric used by [33].

C. Annual Mean Absorbed Power

Equation 6 was used to calculate the Annual Mean Absorbed Power (AMAP) for five different WECs for hindcast, historical ensemble mean meiX, and two future ensemble means me4X and me8X for three different locations (see Tables III, IV, and V). The results compare well with [24].

These WECs are different not only by the maximum power they can provide but also by the combination of H_s and T_e that will make the WEC the most productive. Indeed, if we observe the power matrices of these WECs (see [24] and [31]) we can see that they have very pronounced areas that do not include the whole spectrum of H_s and T_e. For example, F-HBA WEC produces the most power if T_e is 7 s and 11 s and H_s around 4 m and higher. So, if the area of interest has more sea states with these characteristics, then the calculation for F-HBA WEC would show higher values of the Annual Mean Absorbed Power than in the case of an area where these sea states are rarely encountered.

It can be concluded that the highest values of the Annual Mean Absorbed Power for all WECs are obtained in Location 1. In the future, for all locations and all WECs, we can see a decrease in the Annual Mean Absorbed Power ranging from less than 1% to 12% depending on the WEC technology and the location considered. Almost no change from the historical to the future period for the AMAP can be seen in Table IV, with only a small decrease in Table III. The largest decreases of 10% to 12% can be seen for me8X in Table V. Comparing these results to Figure 4, the change in C_gE at Location 2 (near EMEC off the coast of Scotland) is not statistically significant in all seasons, whereas Location 3 off the coast of France has a significant decrease in the mean C_gE across all seasons for both RCP4.5 and RCP8.5.

TABLE III
Annual Mean Absorbed Power at Location 1

AMAP (kW)	PELAMIS	F-3OF	F-2HB	F-OWC	F-HBA
hindcast	279.8	136.2	295.5	346.6	501.1
meiX	284.8	136.1	301	353.9	505.1
me4X	270.3	131.7	285.8	333.8	499.2
me8X	264.7	129.9	279.7	325.8	491.1

TABLE IV
Annual Mean Absorbed Power at Location 2

AMAP (kW)	PELAMIS	F-3OF	F-2HB	F-OWC	F-HBA
hindcast	177.5	99.6	176.8	195.8	321.7
meiX	167.0	93.0	165.9	181.3	294.9
me4X	164.7	92.6	164.6	180.2	294.3
me8X	163.5	91.5	164.0	179.0	294.1

TABLE V
Annual Mean Absorbed Power at Location 3

AMAP (kW)	PELAMIS	F-3OF	F-2HB	F-OWC	F-HBA
hindcast	131.0	116.5	154.0	183.7	373.3
meiX	140.6	121.1	167.7	200.7	398.6
me4X	128.3	113.3	152.1	180.8	364.9
me8X	123.2	109.8	147.2	174.6	356.8

D. Weather Windows and Survivability

By looking at Table VI, Figure 6 and Figure 7, we can see that extreme sea states occur regularly in the Northeast Atlantic even in spring and autumn but especially in the winter period and will continue in the future [19], [27], [34]. The frequency of these extreme events is decreasing for Location 1 and 3 (not shown), which coincides with the results from subsection B. The occurrence of extreme events at Location 2 does not show a clear decrease or increase under the RCP4.5 and RCP8.5 scenarios.

Table VII shows the percentage of time when H_s is less than 1 m and these windows can be used for WEC maintenance (see [21], [35], [36]) if their duration is long enough for marine operations. The duration of these weather windows has not been taken into account, however this will be included in future work. This condition (H_s is less than 1 m) is often satisfied in the spring and autumn but more frequently in the summer. We can see that the frequency of smaller waves occurring will be higher in the future by looking at the annual mean value for me81, me82, and me83 and significantly so in the summer period for Location 1 and 2 (not shown), but less in Location 3 (not shown) which again coincides with the results from subsection B.

E. Extractable Energy / Time Operational Capacity

Location 1 is operational more than 90 % of the time (see Table IX) but that corresponds to only 75 % of the annual wave energy flux available at Location 1 (see Table VIII). This shows that if WECs are not able to extract some of the most energetic sea states (due to issues of survivability and design when sea states are too large), then that part of available ocean energy will be lost for energy production and is not extractable.

There are only slight changes in the future operational capacity in Table IX, with a slight increase in the winter time for Location 1. This coincides with a corresponding

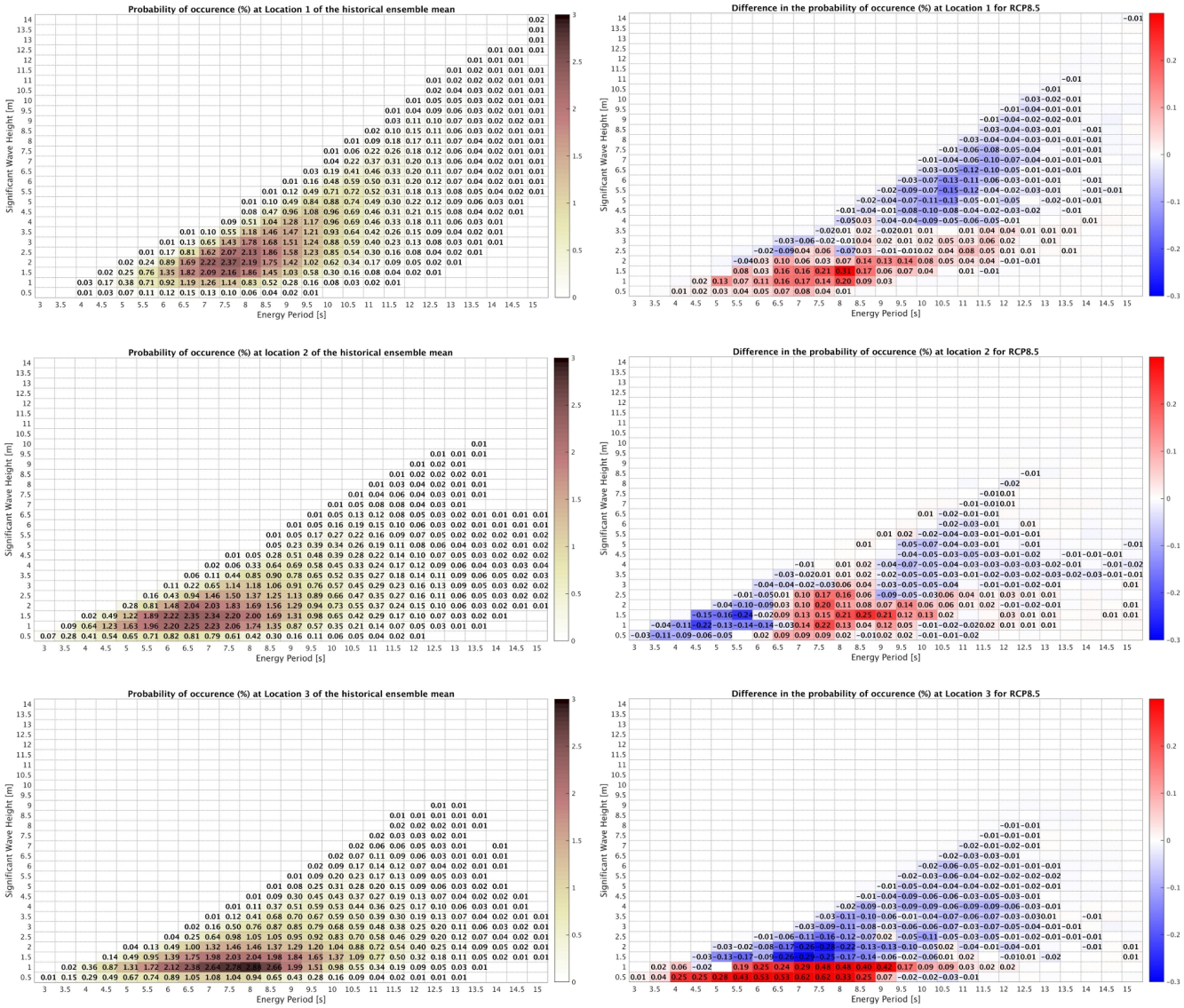

Fig. 5. Left panels: Probability of occurrence scatter diagrams (hourly timeseries of (H_s,T_e)) for Location 1 (top), 2 (middle), and 3 (bottom) for the EC-Earth driven WW3 historical runs (mei1,mei2, mei3), for the period 1980 - 2009. Right panels: Percentage difference in the frequency of occurrence scatter diagrams for Location 1, 2, and 3 for the period 2070 - 2099 under the RCP8.5 scenario (me81, me82, me83).

increase in the C_gE available for extraction in Table VIII in the future period compared to the historical annual mean (due to increases in winter and spring). This is despite an overall decrease of more than 15% in C_gE in the Northeast Atlantic in these regions (see Figure 4). As can be seen in Table VI, there is a drop in the percentage of time where $H_s > 7$ m in winter and spring for the future period, and as these sea states are considered not extractable for the purposes of this study, they do not affect the percentage of time when the WEC is considered to be operational (Table IX). In [19] a $\sim$14% decrease was found off the west coast of Ireland in the 95th percentile of H_s, indicating that projected reductions in the mean wave climate affect higher percentiles to a greater extent. The annual mean percentage of the operational capacity for Location 2 (not shown) is approximately 85 %, while in Location 3 (not shown) it is 75 %. There is a 5 % decrease in the annual mean percentage of the operational capacity for Location 3 in the future. The annual wave energy flux is over 86 % for Location 2 (not shown) and over 90 % for Location 3 (not shown). The annual wave energy flux for both locations does not show a significant change in the future. Figure 8 shows a detailed breakdown by season of the percentage of time C_gE is deemed to be extractable by location. The frequency of occurrence (years) histograms show the variability in the percentage time when $H_s < 1$ m and $H_s > 7$ m. Looking at the left hand panels for Location 1, the time operational capacity never drops below 70% across all seasons and both historical and future periods, whereas there

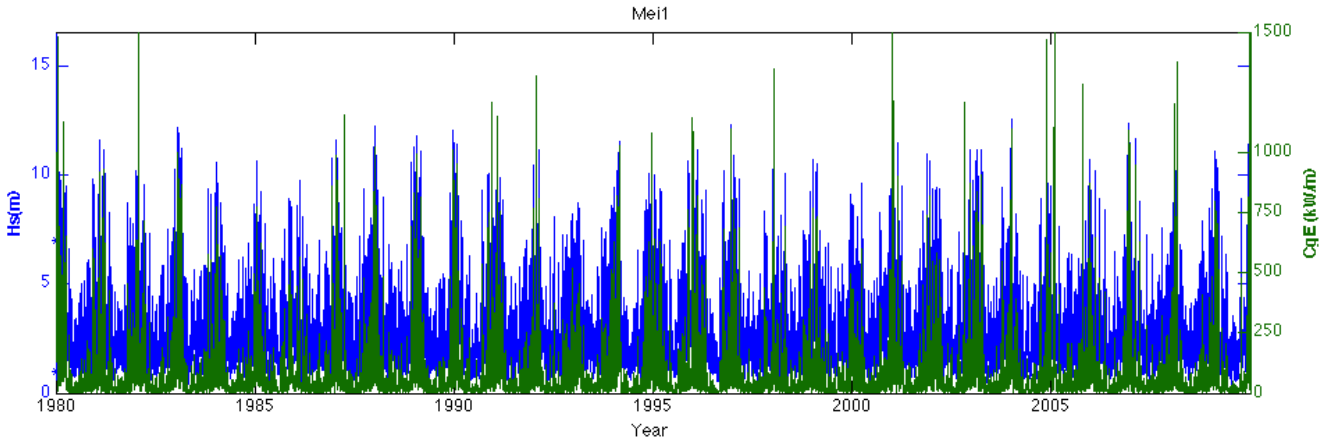

Fig. 6. Timeseries of H_s and C_gE overlaid at Location 1, for mei1 (1980 - 2009). Note: H_s axis on left (blue) and C_gE axis on the right (green).

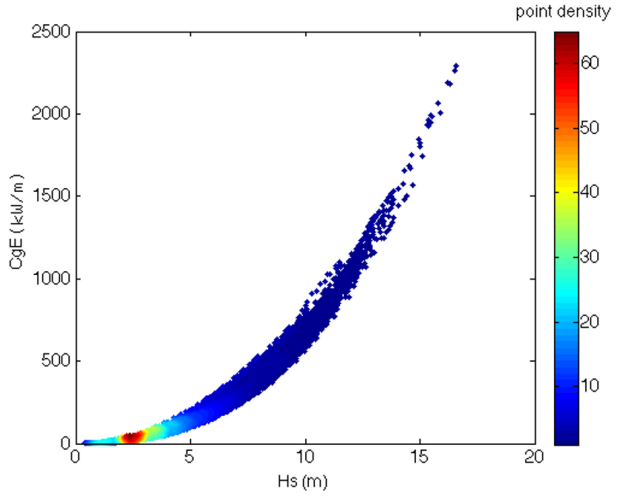

Fig. 7. Scatter plot of H_s versus C_gE at Location 1, for mei1 (1980 - 2009). Large values of C_gE (over 1000 kW/m) can be seen when phenomenal sea states occur ($H_s > 14$ m). Note: in all water depths C_gE is proportional to ${H_s}^2$.

is a marked seasonal variability in Locations 2 and 3, with summer having the lowest time operational capacity, dropping as low as 35% in Location 3.

VI. Conclusions

We carried out an analysis of the future wave climate availability in the Northeast Atlantic under two future Greenhouse Gas emission scenarios, RCP4.5 and RCP8.5, focusing on three locations with potential for future large scale WEC deployment, as shown in Figure 1. Recent studies have found an overall decrease in the wave energy flux off western seaboards in the Northeast Atlantic, particularly under RCP8.5 (see [19], [20], [32], [33], [37]), linked to decreases in 10 m winds over the North Atlantic Ocean, and are consistent with the findings of this study. Changes in the directionality of the wave climate, with seasonal rotations of up to 10° or more in regions in the Northeast Atlantic, have also been found in [32].

Although a significant reduction in the overall wave energy flux towards the end of the century was found in this study, the subsequent change in potential hours of operation remained stable, indicating that the long-term viability of the potential WEC farm locations examined may not be significantly affected. Issues of survivability and access for maintenance remain in more energetic locations.

The probability of occurrence scatter diagrams show decrease in the energetic sea states and an increase in the low energy sea states for Locations 1 and 3, while in Location 2 there is a decrease in both low and high energy sea states and an increase in the mid-ranges.

Annual Mean Absorbed Power tables show a small decrease in Location 1 (1 - 8%), little change (less than 2%) for Location 2 and decreases of 8 - 12% for Location 3 for all WECs in the future across both RCP scenarios. Location 1 shows the highest values of AMAP.

The mean percentage of occurrence of weather windows is the highest in summer with over 30 % for Locations 2 and 3, but only 10 % for Location 1. The annual mean percentage of occurrence of weather windows is around 20 % for Locations 2 and 3 and only around 4 % for Location 1. Accessibility planning for marine operations is essential in the most energetic locations (such as Location 1) where access for installation and maintenance could be severely limited. The mean percentage of occurrence of extreme events (considered $H_s > 7$ m) is the highest in winter with around 2 % for Locations 2 and 3, while up to over 12 % for Location 1. The annual mean percentage of occurrence of extreme events is below 1 % for both Location 2 and 3, but for Location 1 up to 4 %. Finally, Locations 2 and 3 experience lower energy sea states and more weather windows compared to Location 1, which is the most energetic of the locations examined in detail. All locations offer more than 75 % of annual mean time operational capacity and annual wave energy flux.

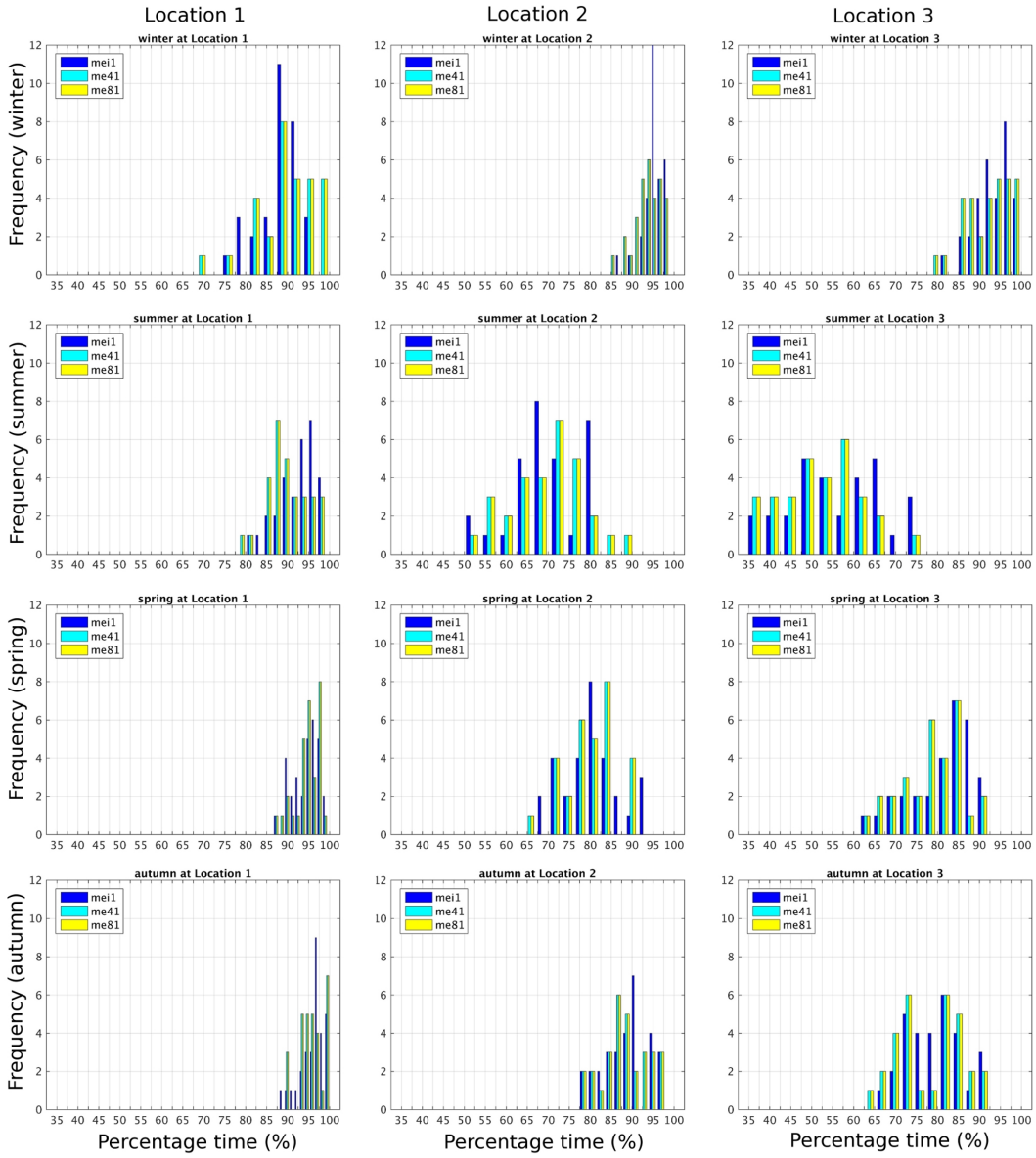

Fig. 8. Frequency of occurrence histogram (years) for the seasonal percentage of time (%) when C_gE is considered extractable by our metric, relative to the total time (30 years of hourly data). Data is displayed for ensemble members mei1 (past), me41, and me81 (future under both RCP4.5 and RCP8.5) for the historical period (1980 - 2009), and the future period (2070 - 2099). C_gE is considered to be available for extraction under the following criteria: i) $H_s > 1$m and ii) $H_s < 7$m.

ACKNOWLEDGMENTS

This work is supported by Science Foundation Ireland (SFI) through Marine Renewable Energy Ireland (MaREI), the SFI Centre for Marine Renewable Energy Research-(12/RC/2302). We thank Emily Gleeson who provided the EC-Earth data. The authors acknowledge Roxana Tiron who helped with the simulations and the Irish Centre for High-End Computing (ICHEC) for the provision of computational facilities. Authors wish to thank anonymous reviewers for their comments and suggestions.

REFERENCES

[1] S. Gallagher, R. Tiron, and F. Dias, "A Long-Term Nearshore Wave Hindcast for Ireland: Atlantic and Irish Sea coasts (1979–2012)," *Ocean Dynamics*, vol. 64, no. 8, pp. 1163–1180, 2014.

[2] S. Gallagher, R. Tiron, E. Whelan, E. Gleeson, F. Dias, and R. McGrath, "The Nearshore Wind and Wave Energy Potential of Ireland: A High Resolution Assessment of Availability and Accessibility," *Renewable Energy*, vol. 88, pp. 494–516, 2016.

[3] R. Atan, J. Goggins, and S. Nash, "A Detailed Assessment of the Wave Energy Resource at the Atlantic Marine Energy Test Site," *Energies*, vol. 9, no. 11, 2016. [Online]. Available: http://www.mdpi.com/1996-1073/9/11/967

[4] B. Drew, A. Plummer, and M. Sahinkaya, "A Review of Wave Energy Converter Technology," pp. 887–902, 2009.

[5] H. Titah-Benbouzid and M. Benbouzid, "Ocean Wave Energy Extraction: Up-To-Date Technologies Review and Evaluation," in *Power Electronics and Application Conference and Exposition (PEAC), 2014 International*. IEEE, 2014, pp. 338–342.

TABLE VI

Percentage of time when $H_s > 7$ m at Location 1 over all ensemble members (nine x 30-year simulations) and the hindcast.

		hindcast	mei1	mei2	mei3	me41	me42	me43	me81	me82	me83
annual	mean	3.24	3.80	4.31	4.11	3.55	3.48	2.97	2.92	2.92	3.16
winter	mean	8.90	11.72	12.55	10.50	10.10	9.82	7.33	8.28	8.00	9.11
spring	mean	1.96	1.85	2.34	2.75	1.70	2.27	2.18	1.65	1.64	1.35
summer	mean	0.02	0.03	0.16	0.09	0.09	0.09	0.03	0.01	0.08	0.08
autumn	mean	1.98	2.10	2.15	3.06	2.13	1.87	2.41	1.96	2.26	2.19

TABLE VII

Percentage of time when $H_s < 1$ m at Location 1 over all ensemble members (nine x 30-year simulations) and the hindcast.

		hindcast	mei1	mei2	mei3	me41	me42	me43	me81	me82	me83
annual	mean	3.50	3.43	3.51	3.66	4.08	4.59	3.77	4.48	4.43	4.56
winter	mean	0.54	0.19	0.38	0.26	0.28	0.32	0.92	0.65	0.68	0.38
spring	mean	3.50	3.79	3.82	4.47	3.79	3.83	3.13	3.39	4.11	3.33
summer	mean	7.67	7.66	7.76	8.25	9.98	11.21	9.53	10.51	10.14	11.79
autumn	mean	2.21	1.97	2.00	1.55	2.16	2.88	1.56	3.26	2.70	2.63

TABLE VIII

Percentage of total C_gE that is available for extracted at Location 1. C_gE is considered: i) extractable - if $H_s > 1$ m and $H_s < 7$ m; ii) too high - if $H_s > 7$ m; and iii) too low - if $H_s < 1$ m.

		hindcast	mei1	mei2	mei3	me41	me42	me43	me81	me82	me83
	high	21.8	26.2	29.0	27.2	26.2	25.0	22.5	22.5	23.2	24.6
annual	extractable	78.1	73.7	70.9	72.6	73.7	74.8	77.3	77.4	76.6	75.2
	low	0.13	0.12	0.12	0.12	0.15	0.17	0.15	0.18	0.17	0.17
	high	32.9	38.5	41.9	37.4	38.7	36.4	31.5	33.2	33.7	36.9
winter	extractable	67.1	61.5	58.1	62.6	61.3	63.6	68.5	66.8	66.3	63.1
	low	0.01	0.00	0.01	0.01	0.01	0.01	0.02	0.02	0.02	0.01
	high	14.7	16.0	20.8	21.0	15.4	19.1	19.3	14.2	15.1	12.9
spring	extractable	85.1	83.8	79.0	78.8	84.4	80.7	80.6	85.6	84.7	87.0
	low	0.17	0.17	0.18	0.19	0.19	0.18	0.15	0.16	0.20	0.17
	high	0.26	0.51	2.65	1.58	1.96	1.76	0.60	0.24	1.65	1.73
summer	extractable	98.8	98.7	96.6	97.5	96.9	96.9	98.3	98.4	97.1	96.8
	low	0.91	0.83	0.79	0.87	1.11	1.38	1.09	1.37	1.21	1.49
	high	13.1	15.5	14.9	20.1	16.4	13.2	17.0	15.0	16.9	15.4
autumn	extractable	86.8	84.4	85.0	79.8	83.5	86.6	83.0	84.9	83.0	84.5
	low	0.09	0.08	0.08	0.06	0.09	0.13	0.07	0.14	0.10	0.10

[6] G. Boyle *et al.*, *Renewable energy: Power for a Sustainable Future*. Taylor & Francis, 1997.

[7] "European Marine Energy Centre," http://www.emec.org.uk/marine-energy/wave-devices/, 2017.

[8] E. Rusu and F. Onea, "Estimation of the Wave Energy Conversion Efficiency in the Atlantic Ocean Close to the European Islands," *Renewable Energy*, vol. 85, pp. 687–703, 2016.

[9] X. Wang, Y. Feng, and V. Swail, "Climate Change Signal and Uncertainty in CMIP5-Based Projections of Global Ocean Surface Wave Heights," *Journal of Geophysical Research: Oceans*, vol. 120, no. 5, pp. 3859–3871, 2015.

[10] K. Taylor, R. Stouffer, and G. Meehl, "An Overview of CMIP5 and the Experiment Design," *Bulletin of the American Meteorological Society*, vol. 93, no. 4, pp. 485–498, 2012.

[11] D. Dee, S. Uppala, A. Simmons, P. Berrisford, P. Poli, S. Kobayashi, U. Andrae, M. Balmaseda, G. Balsamo, P. Bauer *et al.*, "The ERA-Interim Reanalysis: Configuration and Performance of the Data Assimilation System," *Quarterly Journal of the Royal Meteorological Society*, vol. 137, no. 656, pp. 553–597, 2011.

[12] W. Hazeleger, X. Wang, C. Severijns, S. Ştefănescu, R. Bintanja, A. Sterl, K. Wyser, T. Semmler, S. Yang, B. Van den Hurk *et al.*, "EC-Earth V2. 2: Description and Validation of a New Seamless Earth System Prediction Model," *Climate Dynamics*, vol. 39, no. 11, pp. 2611–2629, 2012.

[13] W. Hazeleger, C. Severijns, T. Semmler, S. Ştefănescu, S. Yang, X. Wang, K. Wyser, E. Dutra, J. Baldasano, R. Bintanja *et al.*, "EC-Earth: A Seamless Earth-System Prediction Approach in Action," *Bulletin of the American Meteorological Society*, vol. 91, no. 10, pp. 1357–1363, 2010.

[14] S. Valcke, "OASIS3 User Guide (prism_2-5)," *PRISM support initiative report*, vol. 3, p. 64, 2006.

[15] G. Madec, "NEMO Ocean Engine, Note du Pôle de Modélisation, 27," *Institut Pierre-Simon Laplace (IPSL), France*, 2008.

[16] T. Fichefet and M. Maqueda, "Sensitivity of a Global Sea Ice Model to the Treatment of Ice Thermodynamics and Dynamics," *Journal of*

TABLE IX
Percentage of time when $H_s > 1$ m and $H_s < 7$ m at Location 1, over all ensemble members (nine x 30-year simulations) and the hindcast.

		hindcast	mei1	mei2	mei3	me41	me42	me43	me81	me82	me83
	mean	93.3	92.8	92.2	92.2	92.4	91.9	93.3	92.6	92.6	92.3
annual	max	96.9	95.9	95.8	95.2	97.0	96.1	95.8	96.6	96.3	95.4
	min	89.2	88.1	87.9	88.6	87.8	86.0	90.4	87.4	88.3	87.4
	std	2.1	2.2	2.1	1.6	2.0	2.5	1.7	2.2	2.3	1.8
	mean	90.6	88.1	87.1	89.2	89.6	89.9	91.7	91.1	91.3	90.5
winter	max	99.2	95.6	100.0	97.9	100.0	99.3	98.4	98.9	97.9	99.2
	min	74.8	75.3	78.7	77.3	67.7	76.1	79.4	77.1	79.3	78.6
	std	5.5	4.9	4.7	5.2	7.1	5.2	4.6	5.0	5.0	5.2
	mean	94.5	94.4	93.8	92.8	94.5	93.9	94.7	95.0	94.2	95.3
spring	max	99.3	99.5	100.0	99.0	98.6	99.1	99.6	100.0	99.7	99.8
	min	84.0	86.6	81.3	85.9	87.3	86.7	89.3	82.7	84.3	88.0
	std	3.5	3.2	4.2	3.3	2.9	3.1	2.9	3.4	4.0	3.1
	mean	92.3	92.3	92.1	91.7	89.9	88.7	90.4	89.5	89.8	88.1
summer	max	98.6	99.1	99.5	98.7	98.5	97.4	99.4	97.6	100.0	97.1
	min	80.4	81.4	80.8	81.5	77.9	76.1	81.9	74.7	76.4	72.1
	std	4.5	4.6	4.7	4.1	4.9	5.6	5.1	6.0	4.9	5.7
	mean	95.8	95.9	95.9	95.4	95.7	95.3	96.0	94.8	95.0	95.2
autumn	max	100.0	99.6	99.3	99.8	100.0	99.5	99.9	99.8	99.3	99.6
	min	87.9	88.0	84.2	88.9	90.1	87.0	91.8	88.4	87.0	87.7
	std	2.9	2.9	3.2	2.7	2.9	3.0	1.8	2.7	2.7	2.8

Geophysical Research: Oceans, vol. 102, no. C6, pp. 12 609–12 646, 1997.

[17] R. Moss, W. Babiker, S. Brinkman, E. Calvo, T. Carter, J. Edmonds, I. Elgizouli, S. Emori, L. Erda, K. Hibbard *et al.*, "Towards New Scenarios for the Analysis of Emissions: Climate Change, Impacts and Response Strategies," 2008.

[18] H. Tolman, "The WAVEWATCH III Development Group (2014). User Manual and System Documentation of WAVEWATCH III version 4.18," *Tech. Note 316, NOAA/NWS/NCEP/MMAB*.

[19] S. Gallagher, E. Gleeson, R. Tiron, R. McGrath, and F. Dias, "Wave Climate Projections for Ireland for the End of the 21st Century Including Analysis of EC-Earth winds over the North Atlantic Ocean," *International Journal of Climatology*, vol. 36, no. 14, pp. 4592–4607, 2016. [Online]. Available: http://dx.doi.org/10.1002/joc.4656

[20] S. Gallagher, E. Gleeson, R. Tiron, R. McGrath, and F. Dias, "Twenty-First Century Wave Climate Projections for Ireland and Surface Winds in the North Atlantic Ocean," *Advances in Science and Research*, vol. 13, pp. 75–80, 2016.

[21] S. Gallagher, R. Tiron, and F. Dias, "A Detailed Investigation of the Nearshore Wave Climate and the Nearshore Wave Energy Resource on the West Coast of Ireland," in *ASME 2013 32nd International Conference on Ocean, Offshore and Arctic Engineering*. American Society of Mechanical Engineers, 2013, pp. V008T09A046–V008T09A046.

[22] J. Morim, N. Cartwright, A. Etemad-Shahidi, D. Strauss, and M. Hemer, "Wave Energy Resource Assessment along the Southeast Coast of Australia on the Basis of a 31-Year Hindcast," *Applied Energy*, vol. 184, pp. 276–297, 2016.

[23] Sea Power Ltd., "Our Technology," http://www.seapower.ie/our-technology, 2017.

[24] A. Babarit, J. Hals, M. Muliawan, A. Kurniawan, T. Moan, and J. Krokstad, "Numerical Benchmarking Study of a Selection of Wave Energy converters," *Renewable Energy*, vol. 41, pp. 44–63, 2012.

[25] B. Cahill, "Characteristics of the wave energy resource at the Atlantic marine energy test site," Ph.D. dissertation, University College Cork, 2013.

[26] T. Hiester and W. Pennell, *The Siting Handbook for Large Wind Energy Systems*. Windbooks, 1983.

[27] E. Gleeson, S. Gallagher, C. Clancy, and F. Dias, "NAO and extreme ocean states in the Northeast Atlantic Ocean," *Advances in Science and Research*, vol. 14, pp. 23–33, 2017. [Online]. Available: http://www.adv-sci-res.net/14/23/2017/

[28] S. Barrett, I. Ashton, T. Lewis, and G. Smith, "Spatial & Spectral Variation of Seaways," in *Proceedings of the 8th European Wave and Tidal Energy Conference*, vol. 7, no. 10, 2009.

[29] D. Clabby, A. Henry, M. Folley, and T. Whittaker, "The Effect of the Spectral Distribution of Wave Energy on the Performance of a Bottom Hinged Flap Type Wave Energy Converter," in *ASME 2012 31st International Conference on Ocean, Offshore and Arctic Engineering*. American Society of Mechanical Engineers, 2012, pp. 331–339.

[30] C. Maisondieu and M. Le Boulluec, "Benefits of using a spectral hindcast database for wave power extraction assessment," *The International Journal of Ocean and Climate Systems*, vol. 7, no. 3, pp. 83–87, 2016.

[31] M. Gonçalves, P. Martinho, and C. Soares, "Assessment of Wave Energy in the Canary Islands," *Renewable Energy*, vol. 68, pp. 774–784, 2014.

[32] J. Janjić, S. Gallagher, and F. Dias, "The Future Northeast Atlantic Wave Energy Potential under Climate Change," in *Proceedings of the Twenty-seventh (2017) International Ocean and Polar Engineering Conference, San Francisco, CA, USA, June 25-30*, 2017, pp. 199–206.

[33] M. A. Hemer, Y. Fan, N. Mori, A. Semedo, and X. Wang, "Projected Changes in Wave Climate from a Multi-Model Ensemble," *Nature Climate Change*, vol. 3, no. 5, pp. 471–476, 2013.

[34] C. Clancy, V. Belissen, R. Tiron, S. Gallagher, and F. Dias, "Spatial Variability of Extreme Sea States on the Irish West Coast," in *ASME 2015 34th International Conference on Ocean, Offshore and Arctic Engineering*. American Society of Mechanical Engineers, 2015, pp. V003T02A026–V003T02A026.

[35] M. O'Connor, T. Lewis, and G. Dalton, "Weather Window Analysis of Irish and Portuguese Wave Data with Relevance to Operations and Maintenance of Marine Renewables," in *ASME 2013 32nd International Conference on Ocean, Offshore and Arctic Engineering*. American Society of Mechanical Engineers, 2013, pp. V008T09A068–V008T09A068.

[36] D. Martins, G. Muraleedharan, and C. Guedes Soares, "Analysis on Weather Windows Defined by Significant Wave Height and Wind Speed," *Renewable Energies Offshore*, pp. 91–98, 2015.

[37] O. Aarnes, M. Reistad, . Breivik, E. Bitner-Gregersen, L. Ingolf Eide, O. Gramstad, A. Magnusson, B. Natvig, and E. Vanem, "Projected Changes in Significant Wave Height Toward the End of the 21st century: Northeast Atlantic," *Journal of Geophysical Research: Oceans*, pp. n/a–n/a. [Online]. Available: http://dx.doi.org/10.1002/2016JC012521